S1 Additional figures

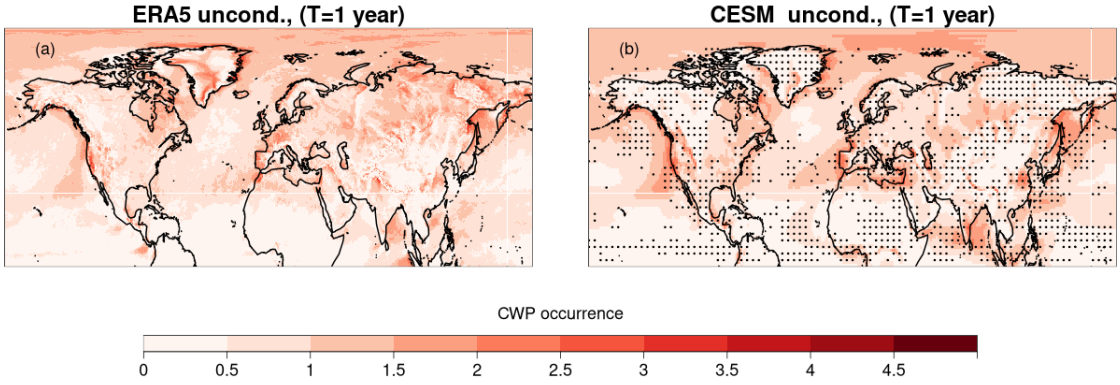

Figure S1. Model evaluation (CESM vs ERA5). ERA5 and CESM mean frequencies (count) of wintertime compound wind and precipitation (CWP) extremes computed at each grid cell without any constraints on modes of variability phases. For model evaluation only, CWP extreme frequencies from the CESM model have been regridded via a nearest-neighbour approach to ERA5 grid. Results are presented by defining CWP extremes when both daily wind and precipitation values exceed their 95th percentiles simultaneously for the period 1959-2019. Numbers in the headers indicate the empirical return period (T=1 year because there are no constraints on modes here in contrast to images in the main text). Stippling indicates that the range of the average CWP extreme frequencies of the CESM ensemble does not cover the value of ERA5.

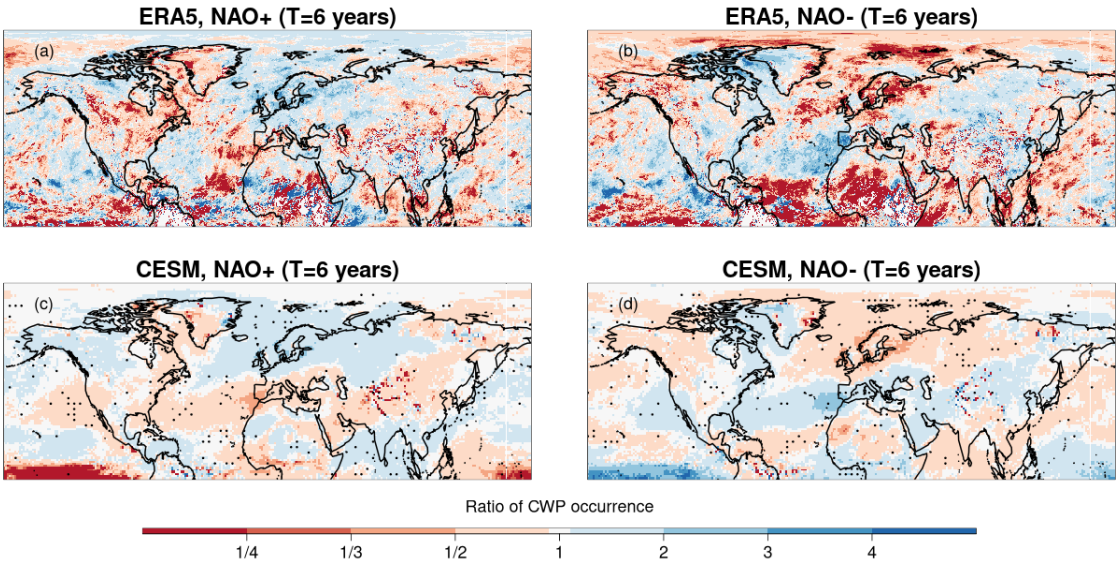

Figure S2. Model evaluation for the effects of NAO. (a, b) ERA5 and (c, d) CESM ratio of mean frequencies of wintertime compound wind and precipitation (CWP) extremes computed at each grid cell between individual phases of the NAO mode and neutral conditions. Please note that here the other modes are not constrained to be in a particular phase due to ERA's limited sample size (see Methods). For model evaluation only, CWP extreme frequencies from the CESM model have been regridded via a nearest-neighbour approach to ERA5 grid. Results are presented by defining CWP extremes when both daily wind and precipitation values exceed their 95th percentiles simultaneously for the period 1959-2019. Numbers in the headers indicate the empirical return periods (in years) for the (a, c) positive and (b, d) negative phases of NAO. Stippling indicates that the range of the ratio of average CWP extreme frequencies for the CESM ensemble does not cover the value of ERA5.

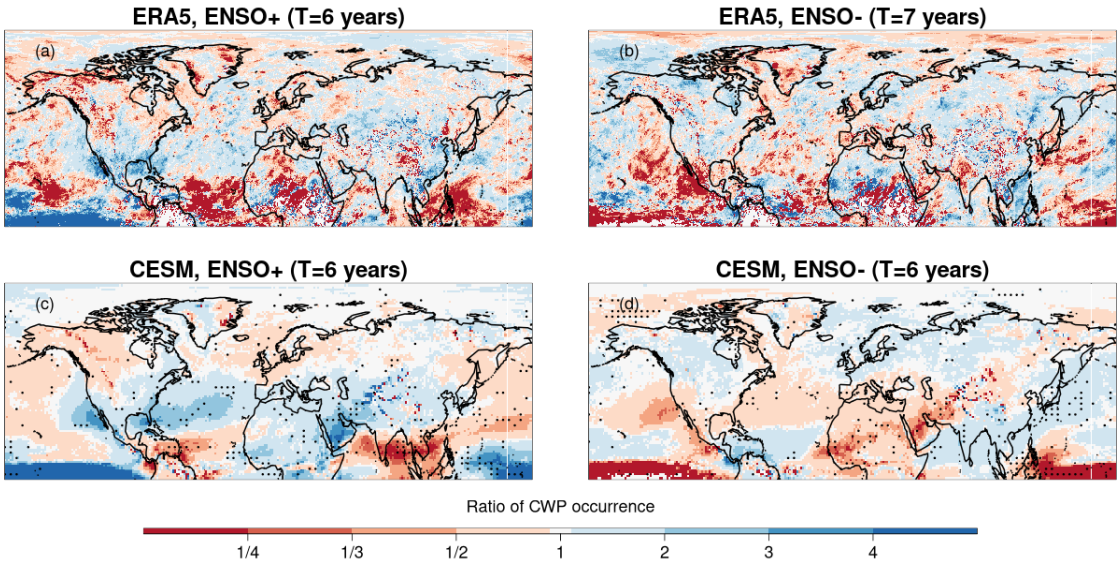

Figure S3. Model evaluation for the effects of ENSO. Same as Fig. S1 but for ENSO.

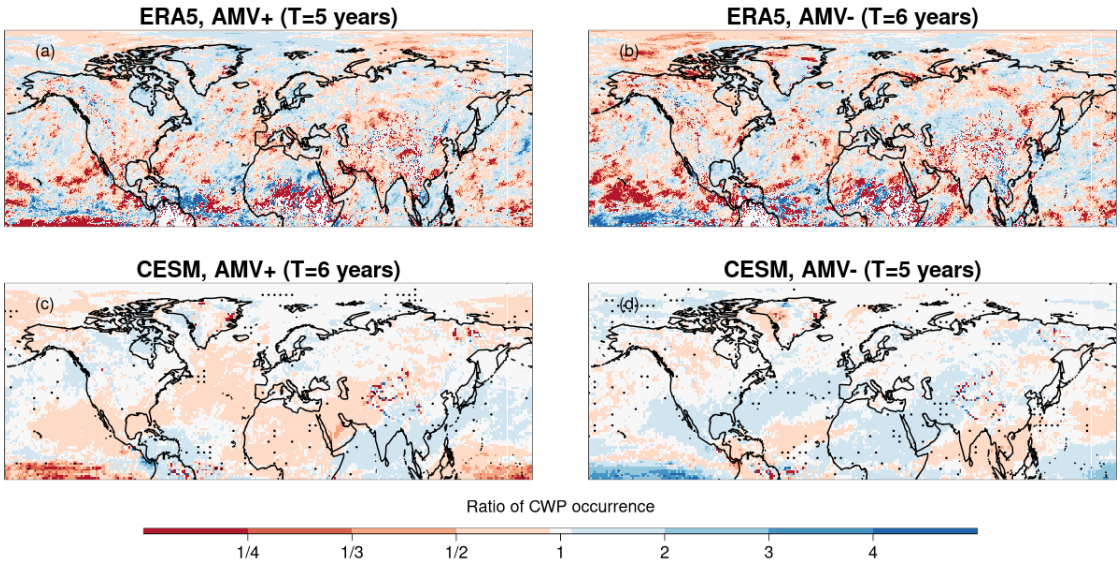

Figure S4. Model evaluation for the effects of AMV. Same as Fig. S1 but for AMV.

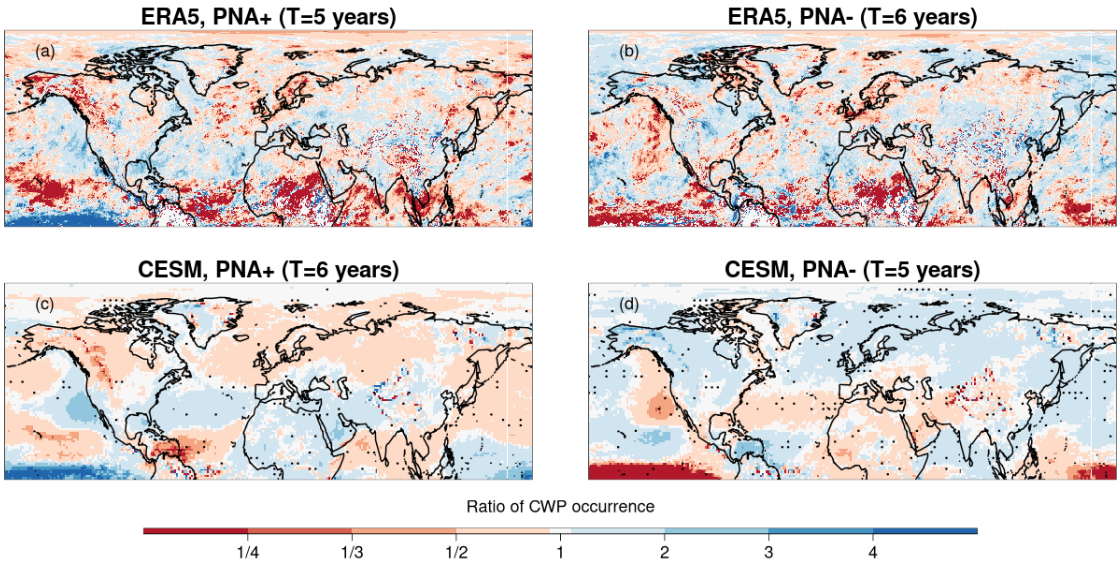

Figure S5. Model evaluation for the effects of PNA. Same as Fig. S1 but for PNA.

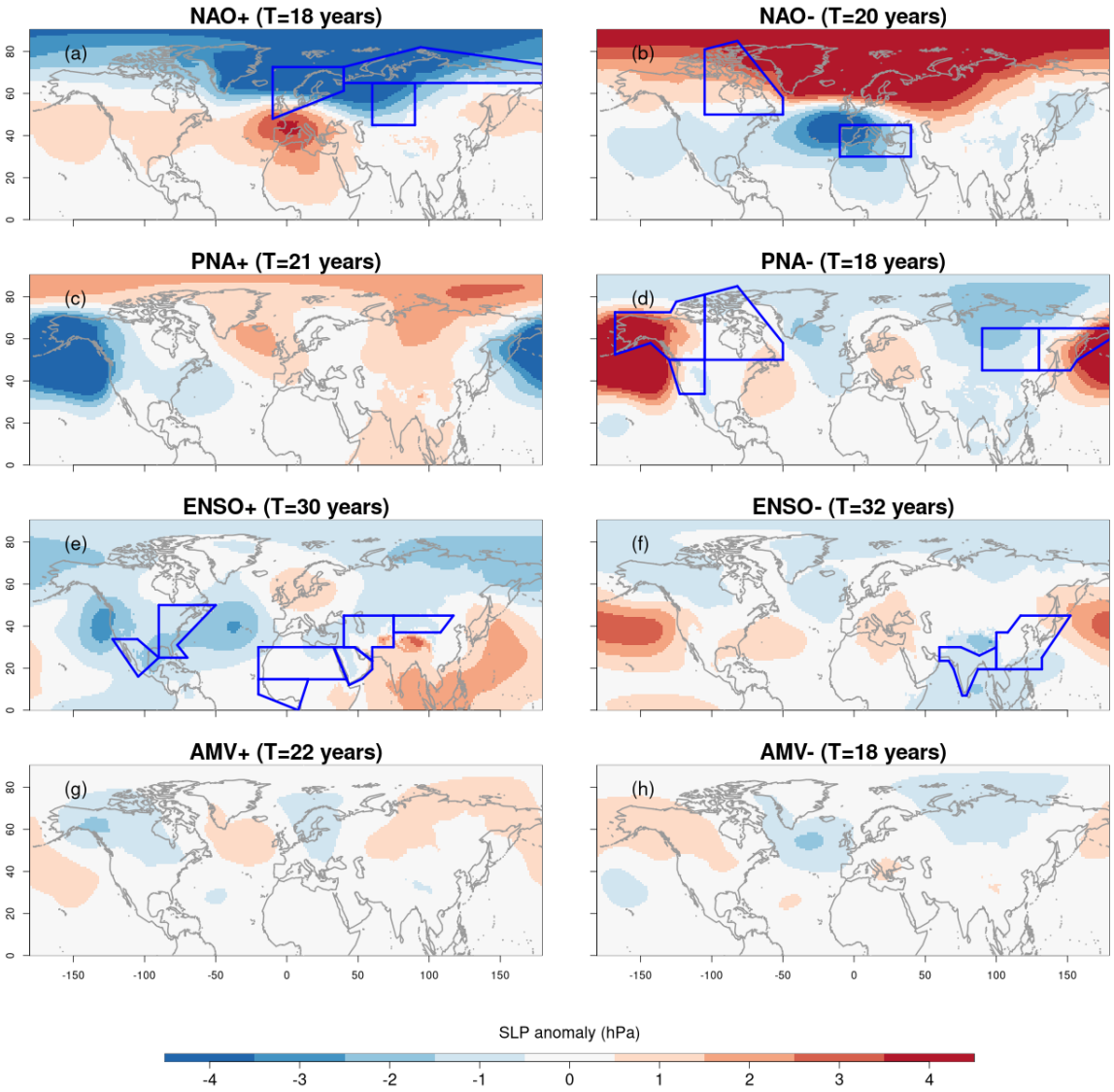

Figure S6. Sea level pressure anomalies for direct effects of variability modes. Mean sea level pressure (SLP) anomalies for the (a) positive and (b) negative phases of NAO (while other variability modes are in their neutral phases) compared to neutral conditions (all variability modes being in their neutral phases) based on the CESM model. Corresponding maps are also displayed for (c, d) PNA, (e, f) ENSO and (g, h) AMV. Numbers in the headers indicate the empirical return period T (in years) for positive and negative phases of the variability modes stated in the title of the panels (while other modes are in their neutral phases). The empirical return period for neutral conditions (i.e., when all modes are in their neutral phases) is T=3 years. The regions framed in blue are areas where the direct effects of variability modes significantly increase regionally averaged compound wind and precipitation extremes compared with neutral conditions (see methods in subsection section 2.2.3); This reflects the information in Fig. 3).

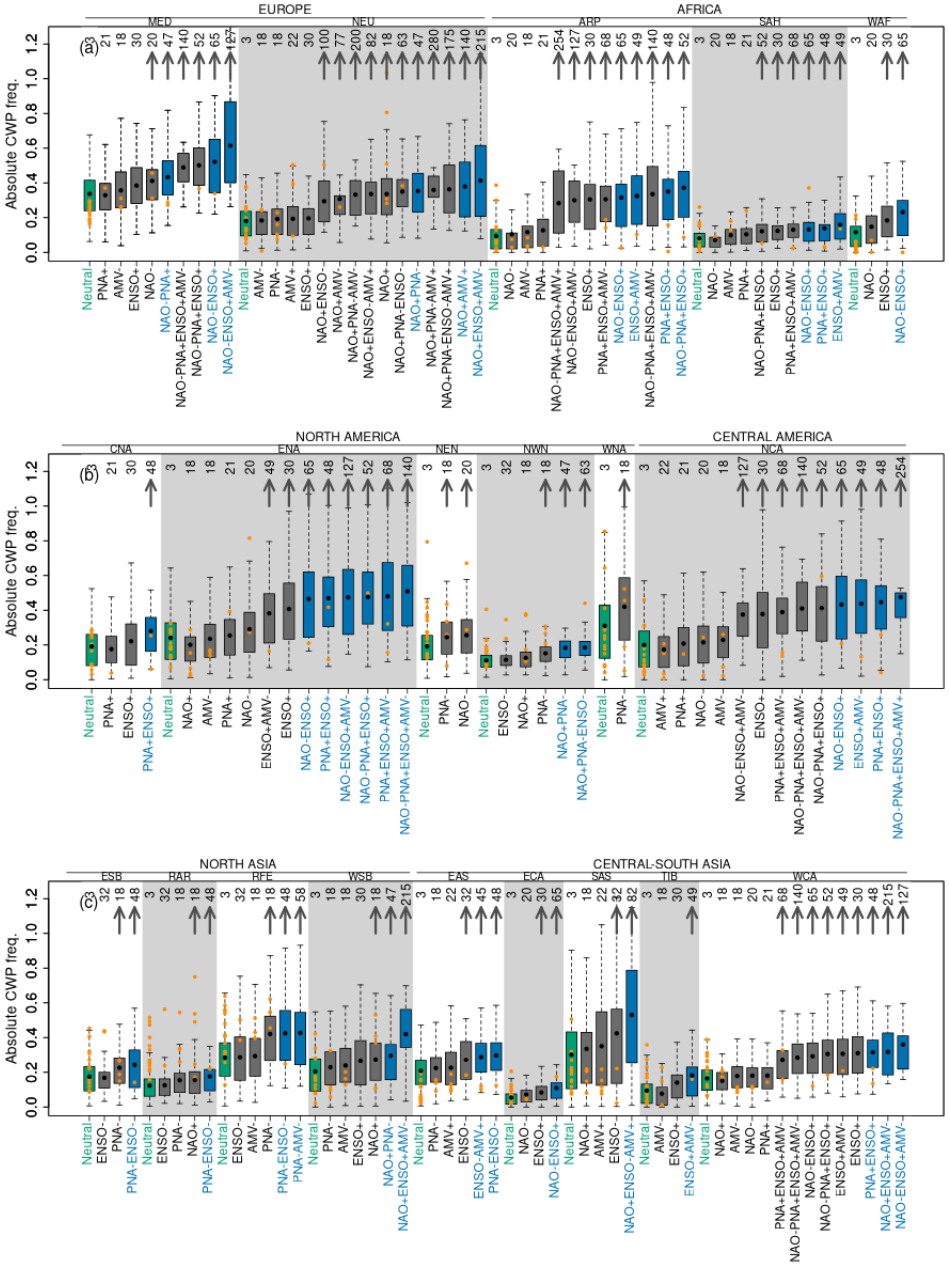

Figure S7. Influence of individual and concurrent variability modes on regional wintertime compound wind and precipitation (CWP) frequency. Same as Fig. 3 but for wintertime absolute frequencies (counts per winter).

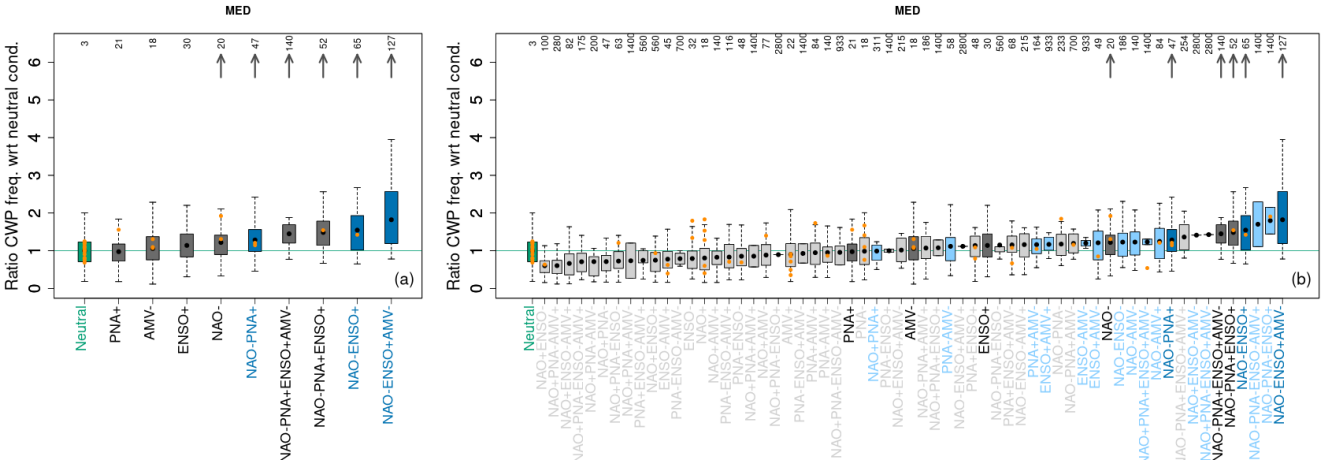

Figure S8. Influence of individual and concurrent variability modes on regional wintertime compound wind and precipitation (CWP) frequency for the MED region. (a) Same as Fig. 3 but for the MED region only. (b) Boxplots for all combinations of modes.

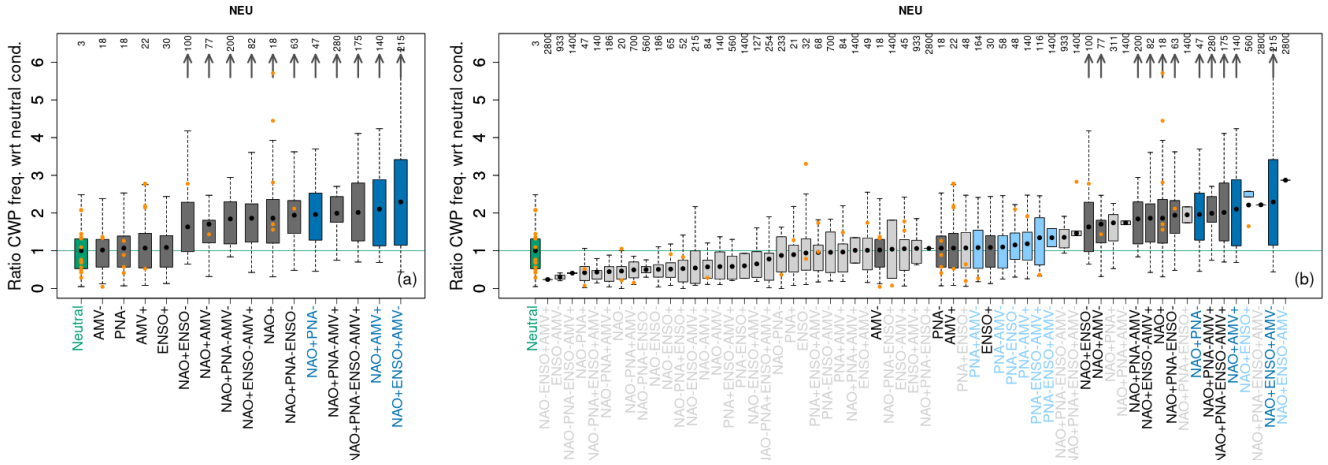

Figure S9. Influence of individual and concurrent variability modes on regional wintertime compound wind and precipitation (CWP) frequency for the NEU region. (a) Same as Fig. 3 but for the NEU region only. (b) Boxplots for all combinations of modes.

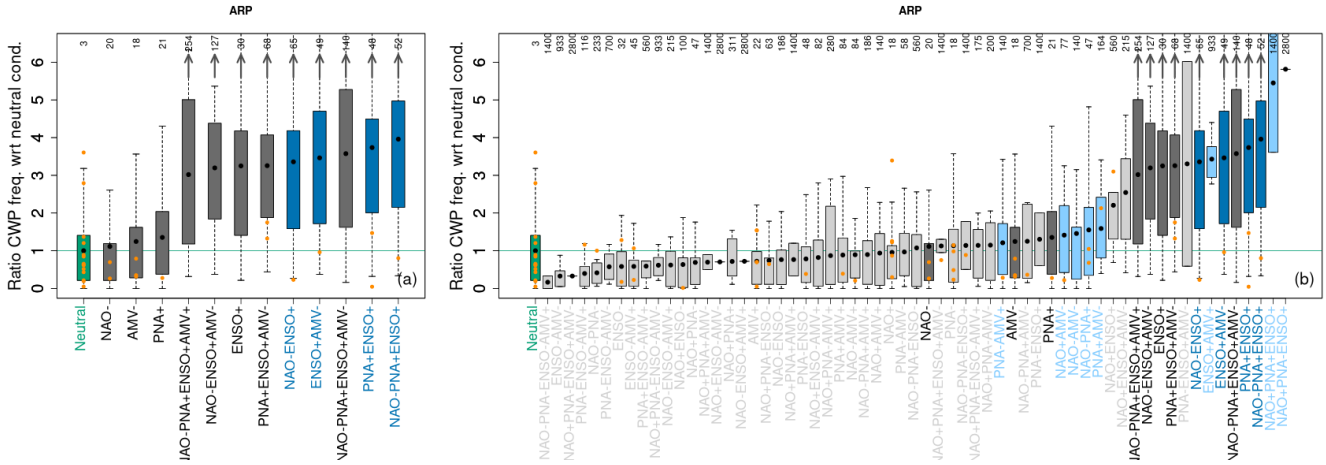

Figure S10. Influence of individual and concurrent variability modes on regional wintertime compound wind and precipitation (CWP) frequency for the ARP region. (a) Same as Fig. 3 but for the ARP region only. (b) Boxplots for all combinations of modes.

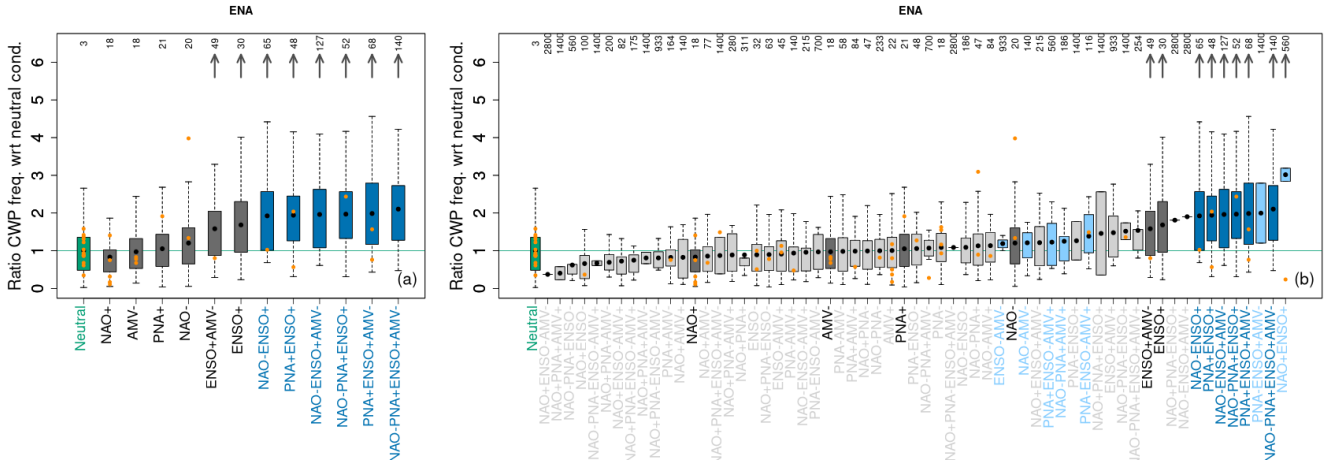

Figure S11. Influence of individual and concurrent variability modes on regional wintertime compound wind and precipitation (CWP) frequency for the ENA region. (a) Same as Fig. 3 but for the ENA region only. (b) Boxplots for all combinations of modes.

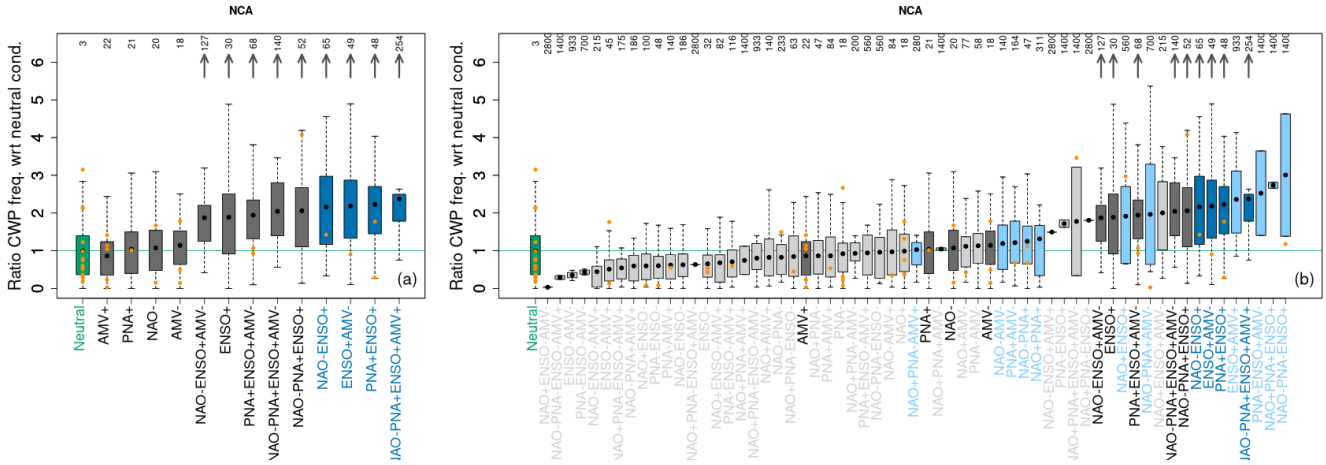

Figure S12. Influence of individual and concurrent variability modes on regional wintertime compound wind and precipitation (CWP) frequency for the NCA region. (a) Same as Fig. 3 but for the NCA region only. (b) Boxplots for all combinations of modes.

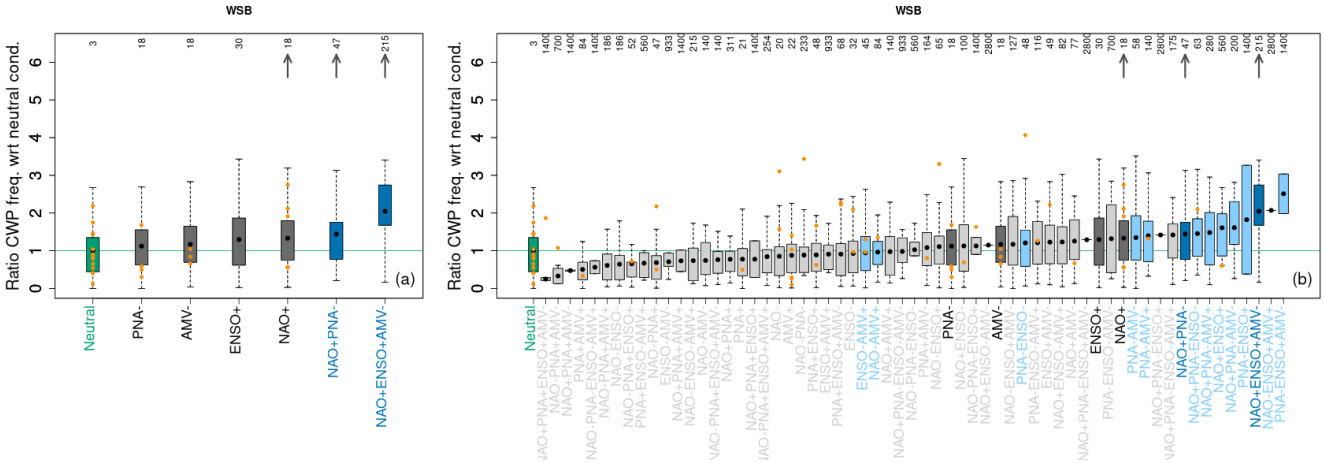

Figure S13. Influence of individual and concurrent variability modes on regional wintertime compound wind and precipitation (CWP) frequency for the WSB region. (a) Same as Fig. 3 but for the WSB region only. (b) Boxplots for all combinations of modes.

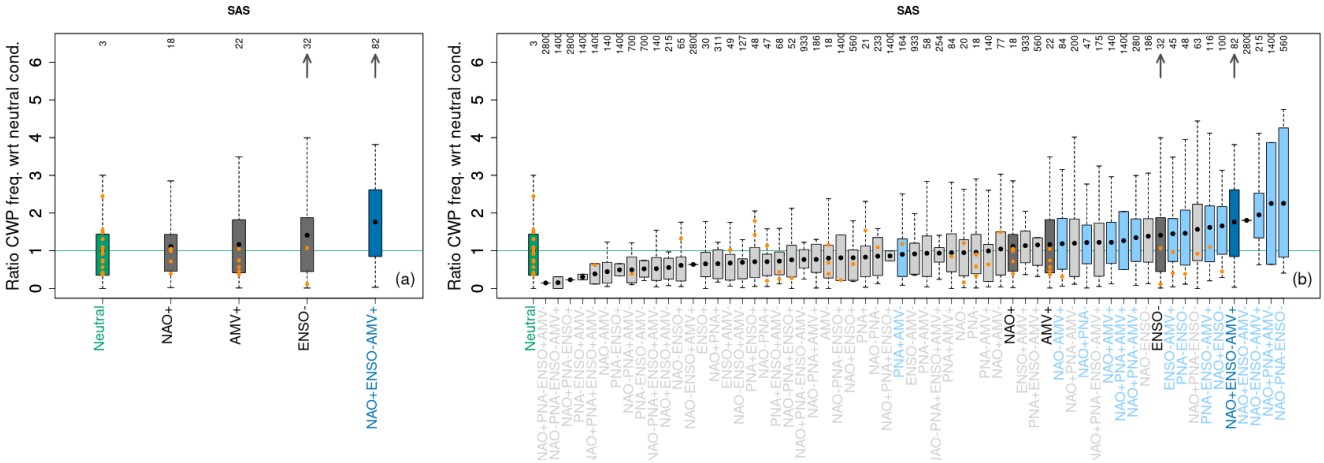

Figure S14. Influence of individual and concurrent variability modes on regional wintertime compound wind and precipitation (CWP) frequency for the SAS region. (a) Same as Fig. 3 but for the SAS region only. (b) Boxplots for all combinations of modes.

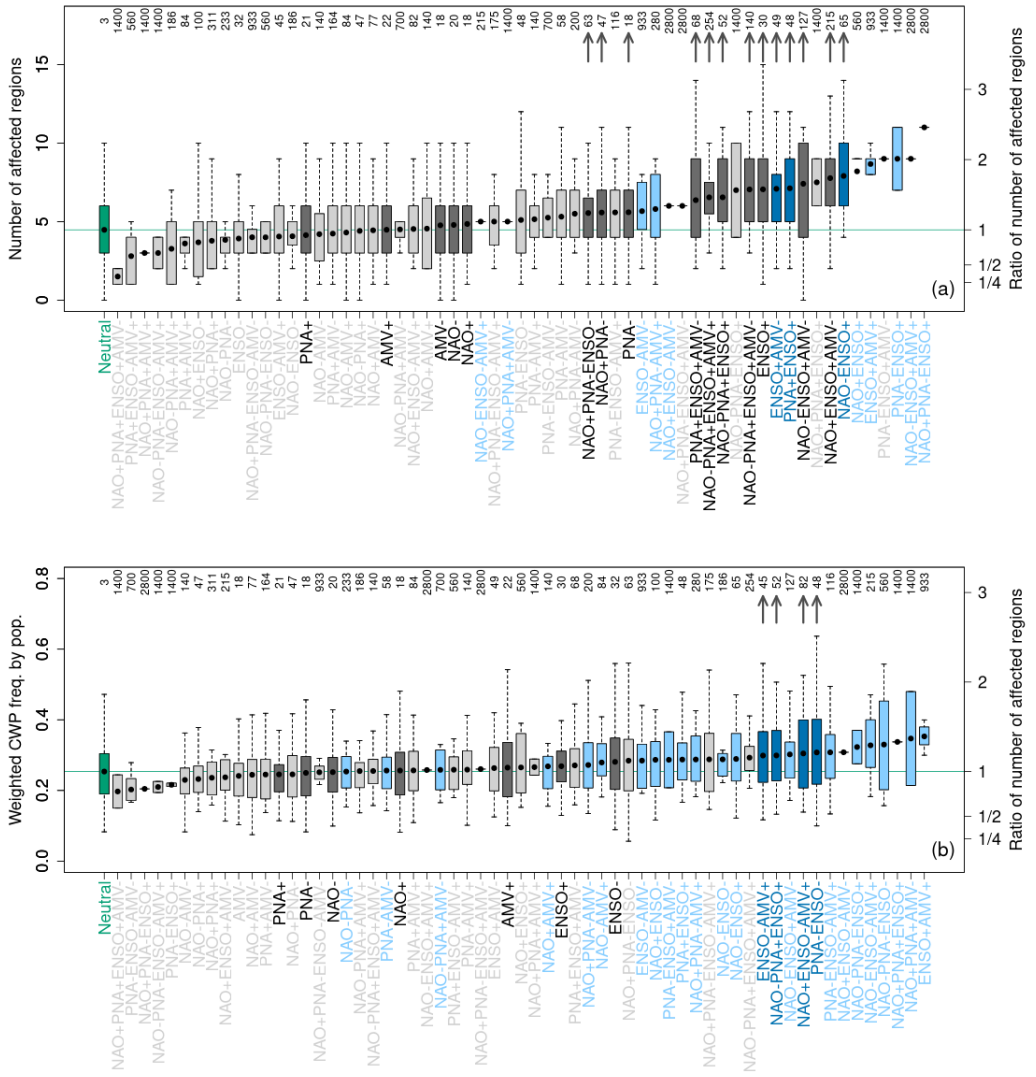

Figure S15. Influence of individual and concurrent variability modes on spatially compounding wind and precipitation (CWP) extremes. Same as Fig. 6 but for all combinations of modes. Light grey and blue colours show distributions of metrics for combinations of modes that are not retained following the methodology.

Table S1. Summary of direct effect of modes of variability on wintertime compound wind and precipitation (CWP) extremes. Blue ticks indicate where the direct effects of modes significantly increase the average wintertime CWP extreme frequencies compared with neutral conditions. Green ticks indicate where those significant direct effects of modes are supported by previous literature.

Regions	Sub-regions	NAO+	NAO-	PNA+	PNA-	ENSO+	ENSO-	AMV+	AMV-
EUROPE	EEU	✓[1]							
	MED		✓✓[2]						
	NEU	✓✓[1]							
	WCE	✓[1]							
AFRICA	ARP					✓✓[3]			
	SAH					✓			
	WAF					✓			
NORTH AMERICA	CNA								
	ENA					✓✓[4]			
	GIC								
	NEN		✓		✓✓[5]				
	NWN				✓✓[5]				
	WNA				✓✓[5]				
C.AM.	CAR								
	NCA					✓✓[6]			
	SCA								
NORTH AS.	ESB				✓				
	RAR	✓✓[7]							
	RFE				✓				
	WSB	✓✓[7]							
C.-S.ASIA	EAS						✓✓[8]		
	ECA					✓			
	SAS						✓✓[9]		
	TIB								
	WCA					✓			

[1] Hurrell and Deser (2010)
[2] Pinto et al. (2009)
[3] Niranjan Kumar and Ouarda (2014)
[4] Yeh et al. (2018)
[5] Guan and Waliser (2015)
[6] Taschetto et al. (2020)
[7] Pinto and Raible (2012)
[8] Zhang et al. (2012)
[9] Mahala et al. (2015)

References

Guan, B. and Waliser, D. E.: Detection of atmospheric rivers: Evaluation and application of an algorithm for global studies, Journal of Geophysical Research: Atmospheres, 120, 12 514–12 535, https://doi.org/10.1002/2015JD024257, 2015.

Hurrell, J. W. and Deser, C.: North Atlantic climate variability: The role of the North Atlantic Oscillation, Journal of Marine Systems, 79, 231–244, https://doi.org/10.1016/j.jmarsys.2009.11.002, impact of climate variability on marine ecosystems: A comparative approach, 2010.

Mahala, B. K., Nayak, B. K., and Mohanty, P. K.: Impacts of ENSO and IOD on tropical cyclone activity in the Bay of Bengal, natural Hazards, 75, 1105–1125, https://doi.org/10.1007/s11069-014-1360-8, 2015.

Niranjan Kumar, K. and Ouarda, T.: Precipitation variability over UAE and Global SST Teleconnections, Journal of Geophysical Research: Atmospheres, 119, https://doi.org/10.1002/2014JD021724, 2014.

Pinto, J. and Raible, C.: Past and recent changes in the North Atlantic oscillation, Wiley interdisciplinary reviews: Climate Change, 3, 79 – 90, https://doi.org/10.1002/wcc.150, 2012.

Pinto, J. G., Zacharias, S., Fink, A. H., Leckebusch, G. C., and Ulbrich, U.: Factors contributing to the development of extreme North Atlantic cyclones and their relationship with the NAO, Climate Dynamics, 32, 711–737, https://doi.org/10.1007/s00382-008-0396-4, 2009.

Taschetto, A., Ummenhofer, C., Stuecker, M., Dommenget, D., Ashok, K., Rodrigues, R., and Yeh, S.-W.: ENSO Atmospheric Teleconnections, pp. 309–335, ISBN 9781119548164, https://doi.org/10.1002/9781119548164.ch14, 2020.

Yeh, S.-W., Cai, W., Min, S.-K., McPhaden, M. J., Dommenget, D., Dewitte, B., Collins, M., Ashok, K., An, S.-I., Yim, B.-Y., and Kug, J.-S.: ENSO Atmospheric Teleconnections and Their Response to Greenhouse Gas Forcing, Reviews of Geophysics, 56, 185–206, https://doi.org/10.1002/2017RG000568, 2018.

Zhang, W., Graf, H.-F., Leung, Y., and Herzog, M.: Different El Niño Types and Tropical Cyclone Landfall in East Asia, Journal of Climate, 25, 6510 – 6523, https://doi.org/10.1175/JCLI-D-11-00488.1, 2012.